Indian Journal of Chemistry
Vol. 65, June 2026, pp. 564-585
DOI: 10.56042/ijc.v65i6.16313

DFT, wave function analyses of protocatechualdehyde, a natural product

J Jebasingh Kores[a], D Abiya Chelliah*[b], J Winfred Jebaraj[c], I Antony Danish[d], S Darwin Paul Edison[b], D Jebixon Immanuel[c], P Jeya Sheela[e] & T Sasitha[c]

[a] Department of Physics, Pope's College[†] (Autonomous), Sawyerpurram 628 251, Tamil Nadu, India
[b] Department of Botany, St. John's College[†], Tirunelveli 627 002, Tamil Nadu, India
[c] Department of Chemistry, St. John's College[†], Tirunelveli 627 002, Tamil Nadu, India
[d] Department of Chemistry, Sadakathullah Appa College[†] (Autonomous), Tirunelveli 627 011, Tamil Nadu, India
[e] Department of Microbiology, Sadakathullah Appa College[†] (Autonomous), Tirunelveli 627 011, Tamil Nadu, India

E-mail: abiya.bot@stjohnscollege.edu.in

Received 10 January 2025; accepted (revised) 10 June 2026

Protocatechualdehyde (3,4-dihydroxybenzaldehyde) is a structurally familiar molecule. In its structure, an electron-withdrawing moiety (–CHO) and two electron donor groups (–OH) are present at neighbouring positions. A bridge and π-linker (aromatic ring) interconnect them. As a consequence, electrons may travel from the donor to the acceptor through the bridge. Gaussian 16W has been employed for all investigations on the DFT/B3LYP/6-311++G(d,p) basis set. MEP analysis predicts that the molecule has electrophilic and nucleophilic domains. Frontier energy gap analysis implies that the molecule is hard and stable. The NBO analysis reports the same results. The IEFPCM solvation effect has been studied for MEP, Mulliken charge, FMO, and UV-Vis spectra. The shaded surface map, NCI, STM, and electron transport studies have been conducted using the Multiwfn 3.8 software. The electron transport analysis results reveal that charge transfer is possible in the S0 → S4, S9, and S10 excitation states. The molecular docking study has been conducted using PyRx. *In silico* toxicity analysis and activity predictions, along with comparisons, have been performed using EPA, DSS, TOX and PASS, respectively.

Keywords: Protocatechualdehyde, DFT, NBO, NCI, Hole-electron transport, Toxicity analysis

Protocatechualdehyde (PCA), also known as 3,4-dihydroxybenzaldehyde is an important class of naturally occurring polyphenol[1]. PCA is found to be widely distributed in barley[2], green cavandish bananas[3] and grapevine leaves[4]. PCA is found to possess antioxidant properties which is isolated from *S. lincolnensis*, as a butanol fraction extract[5]. PCA is a possible new HDAC inhibitor that has anti-cancer effect by downregulating cyclin D1 and HDAC2 in human colorectal cancer cells[6]. It has been demonstrated to have potent antibacterial action against R. solanacearum and to be a useful antibacterial agent for reducing the bacterial wilt that R. solanacearum causes in tobacco[7]. Additionally, *via* activating GPER-1, PCA has been shown to decrease endothelial dysfunction and atherosclerosis both *in vitro* and *in vivo*[8]. 3,4-Dihydroxybenzaldehyde has been utilized as a precursor to prepare Urushiol as an anticorrosive agent[9] and as magnetic covalent organic frameworks[10]. Even though PCA is believed to have multiple biological and synthetic applications, DFT research is only available for tellurium and mercury compounds[11]. Based on the limited work on the analysis of the molecule, it is felt worthwhile to study the intrinsic structural aspects of PCA through density function theory (DFT) to explore the HOMO-LUMO results, NBO, Fukui function analyses, *etc*.

DFT is a popular and generally recognized technique for evaluating a molecule's findings. The electronic structure of atoms, molecules, and solids may also be ascertained using it. It has developed into a fairly comprehensive method for examining the characteristics and composition of molecules. It assures a significant increase in computational accuracy without increasing computational time. According to a review of the literature, there have been no quantitative reports about this wonderful, very important molecule, and hence it is decided to carry out research on this molecule.

† Affiliated to Manonmaniam Sundaranar University, Abishekapatti, Tirunelveli 627 012, Tamil Nadu, India

Computational details

All of the computations for this work are performed using the 6-311++G(d,p) basis set and the Becke–Lee–Yang–Parr hybrid exchange-correlation three-parameter functional (B3LYP) with the aid of Gaussian 16W software[12-14]. The structure is drawn virtually in the Chemsketch software and subjected to optimisation with the help of the Avogadro tool[15,16]. The Gaussview 06 is used to view the molecules after the calculations are performed[17]. The initial structure in the gaseous phase is subjected to optimisation with the help of the above basis set. The complete optimisation and full convergence of the molecule are confirmed by the GaussSum 03 program[18]. Also, IEFPCM (Integral Equation Formalism Polarizable Continum Model) solvation effect for UV-Vis spectra is analysed using the above mentioned tool[18]. The complete optimisation is further confirmed by the absence of negative frequencies. The Multiwfn 3.8 software is used to investigate wave function analysis like NCI, shaded surface map projection with LOL, *etc*[19]. The VMD 1.9.4 software is used to determine the isosurface of the molecule[20]. The PyRx tool is used for the docking studies[21]. EPA DSS TOX is used for *in silico* toxicity analysis[22] and PASS is used for the prediction of biological activity[23].

Materials and Methods

Since PCA is a 97% pure molecule, it is acquired from Sigma Aldrich and utilized as such.

Instrumentation data

Using KBr Pellets (AR) with a diamond crystal plane, a Nicolet 1S5R FT-IR spectrophotometer logs the FT-IR spectra for the title molecule in the 4000-400 cm^{-1} range. A double-beam UH-5300 spectrophotometer (Hitachi) records the UV-Vis spectrum after 0.5 mg of the sample is dissolved in 10 mL of 100% ethanol to create the sample with the required concentration.

Results and Discussion

Geometry and electronic structure analysis

Since there are two –OH groups present at neighbouring carbon atoms, the following conformers are possible (Fig. 1). Hence, conformational analysis is carried out to identify the conformer with the least energy. For this molecule, the conformer (3) is chosen for further research since it has the lowest energy (-496.1686281 a.u.). The complete optimisation of the selected conformer is confirmed by the GaussSum 03 tool, and the picture is given in Fig. 1. The list of atoms in the target molecule is given in Table 1.

The DFT/B3LYP/6-311++G(d,p) basis set has been employed to evaluate the electronic structure of

Table 1 — List of atoms of the optimized target molecule

1	2	3	4	5	6	7	8
C	C	C	C	C	C	C	O
9	10	11	12	13	14	15	16
O	O	H	H	H	H	H	H

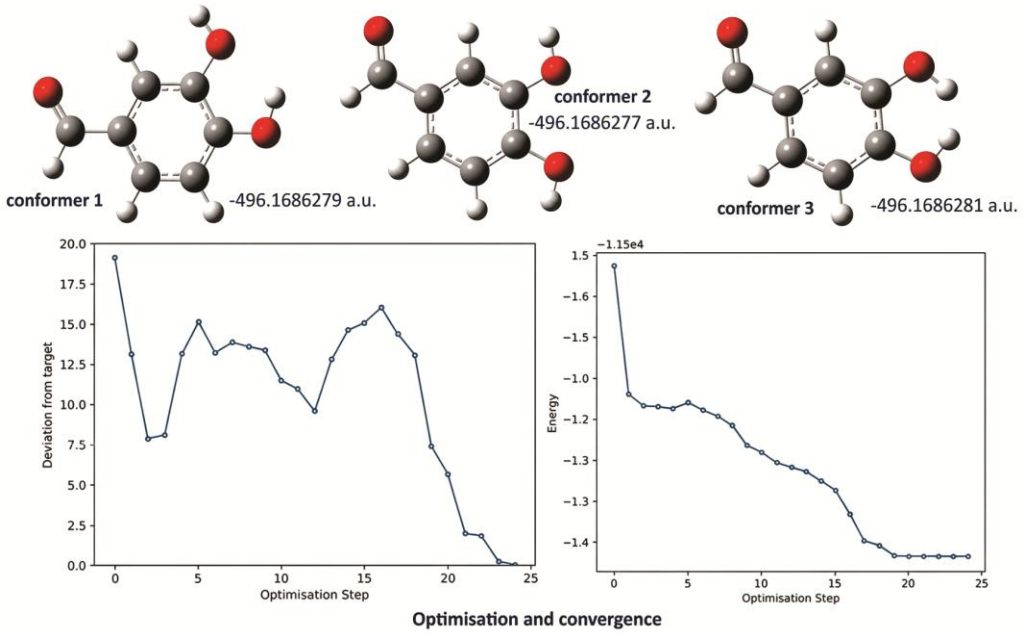

Fig. 1 — Geometry and optimisation of the conformers (1-3), with energies and images of optimisation and convergence of PCA

the object of study in the gaseous phase. The findings are replicated in Table 2. "The bond distance is defined as the average distance between the nuclei of two bonded atoms in a molecule". For this molecule, the shortest bond length is identified at 8O-15H (0.963 Å) while the longest bond distance is located at 1C-7C (1.472 Å). The average angle between the orbitals around the central atom of a molecule that contains bonding electron pairs is known as the bond angle. In this study, the shortest bond angle is seen at 4C-9O-16H (108.7°) and the largest bond angle is observed at 1C-7C-10O (125.1°). "The dihedral angle is defined as the angle between two planes, both of which pass through the same bond". In this present investigation, the dihedral angle reveals that the molecule is planar. V. Balachandran *et.al.* have investigated some parameters about 2,3-dihydroxybenzaldehyde, and the present investigation matches the literature values[24].

Mulliken population analysis

The aforementioned level of theory is applied to calculate the Mulliken population analysis for the target molecule in a variety of solvents, including water, ethanol, THF, DMSO, and benzene. The charge distribution is tabulated in Table 3. A graph is also generated and displayed in Fig. 2.

It is evident from Fig. 2 that the attachment of an electron-withdrawing group makes 1C more positive than any other atom for the title molecule in the gaseous phase. 5C has a very low value (-1.6784 a.u.). The charges on 8O, 9O, and 10O are -0.3016, -0.2259, and -0.2602 a.u. respectively. All the hydrogen atoms are being positive in which 14H is having very low value (0.1300 a.u.) and 16H has more value (0.2890 a.u.). Intramolecular hydrogen bonding may result from the presence of a positive charge on hydrogen atoms and a negative charge on oxygen atoms[25]. In Fig. 2, the Mulliken charges for

Table 2 — The electronic structure of the optimized molecule (in gaseous phase)

S. No	Atom set	Bond length (Å)	Atom set	Bond angle (°)	Atom set	Dihedral angle (°)
1	1C-2C	1.405	2C-1C-5C	119.7	5C-1C-2C-3C	0.0
2	1C-5C	1.398	2C-1C-7C	120.2	5C-1C-2C-11H	180.0
3	1C-7C	1.472	5C-1C-7C	120.1	7C-1C-2C-3C	–180.0
4	2C-3C	1.379	1C-2C-3C	119.7	7C-1C-2C-11H	0.0
5	2C-11H	1.086	1C-2C-11H	118.8	2C-1C-5C-6C	0.0
6	3C-4C	1.410	3C-2C-11H	121.4	2C-1C-5C-12H	180.0
7	3C-8O	1.375	2C-3C-4C	120.5	7C-1C-5C-6C	180.0
8	4C-6C	1.391	2C-3C-8O	125.0	7C-1C-5C-12H	0.0
9	4C-9O	1.354	4C-3C-8O	114.5	2C-1C-7C-10O	0.0
10	5C-6C	1.391	3C-4C-6C	119.8	2C-1C-7C-14H	–180.0
11	5C-12H	1.085	3C-4C-9O	120.3	5C-1C-7C-10O	–180.0
12	6C-13H	1.083	6C-4C-9O	119.9	5C-1C-7C-14H	0.0
13	7C-10O	1.214	1C-5C-6C	120.6	1C-2C-3C-4C	0.0
14	7C-14H	1.110	1C-5C-12H	119.6	1C-2C-3C-8O	–180.0
15	8O-15H	0.963	6C-5C-12H	119.8	11H-2C-3C-4C	–180.0
16	9O-16H	0.967	4C-6C-5C	119.7	11H-2C-3C-8O	0.0
17			4C-6C-13H	118.6	2C-3C-4C-6C	0.0
18			5C-6C-13H	121.7	2C-3C-4C-9O	180.0
19			1C-7C-10O	125.1	8O-3C-4C-6C	180.0
20			1C-7C-14H	114.5	8O-3C-4C-9O	0.0
21			10O-7C-14H	120.5	2C-3C-8O-15H	0.0
22			3C-8O-15H	110.8	4C-3C-8O-15H	180.0
23			4C-9O-16H	108.7	3C-4C-6C-5C	0.0
24					3C-4C-6C-13H	-180.0
25					9O-4C-6C-5C	-180.0
26					9O-4C-6C-13H	0.0
27					3C-4C-9O-16H	0.0
28					6C-4C-9O-16H	-180.0
29					1C-5C-6C-4C	0.0
30					1C-5C-6C-13H	180.0
31					12H-5C-6C-4C	-180.0
32					12H-5C-6C-13H	0.0

Table 3 — Mulliken population analysis of the target molecule

Atoms	Charge (a.u.)					
	Air	Water	Ethanol	THF	DMSO	Benzene
1C	1.4548	1.0098	1.0107	1.0132	1.0107	1.0196
2C	–0.0845	0.1654	0.1653	0.1648	0.1653	0.1626
3C	0.0101	–0.3542	–0.3554	–0.3592	–0.3554	–0.3680
4C	–0.6943	0.0769	0.0755	0.0713	0.0755	0.0614
5C	–1.6784	–1.2297	–1.2274	–1.2205	–1.2274	–1.2036
6C	0.6379	–0.1655	–0.1637	–0.1578	–0.1637	–0.1432
7C	–0.0701	–0.0199	–0.0208	–0.0234	–0.0208	–0.0292
8O	–0.3016	–0.2456	–0.2438	–0.2380	–0.2438	–0.2231
9O	–0.2259	–0.2256	–0.2242	–0.2199	–0.2242	–0.2082
10O	–0.2602	–0.3283	–0.3247	–0.3134	–0.3247	–0.2845
11H	0.1601	0.2100	0.2108	0.2129	0.2108	0.2162
12H	0.1323	0.1790	0.1775	0.1726	0.1775	0.1607
13H	0.2138	0.2203	0.2191	0.2155	0.2191	0.2061
14H	0.1300	0.1823	0.1800	0.1729	0.1800	0.1554
15H	0.2870	0.2635	0.2616	0.2554	0.2616	0.2396
16H	0.2890	0.2614	0.2595	0.2535	0.2595	0.2380

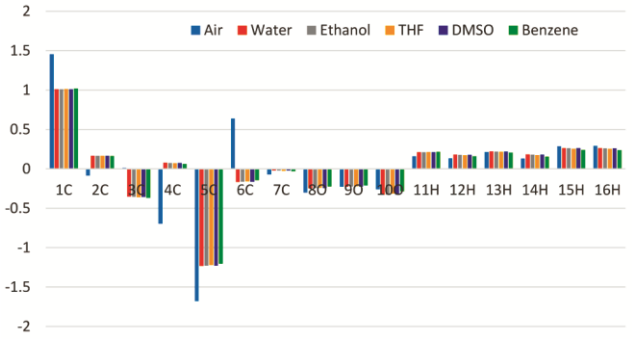

Fig. 2 — Mulliken population diagram for the target molecule in various solvents

various solvents, *viz*. water, ethanol, THF, DMSO, and benzene, are also reported. According to cumulative reports, the title molecule's Mulliken charge is low in the benzene solvent and high in the gaseous phase. All the other solvents exhibit almost the same values.

MEP analysis

The force exerted on an optimistic test charge (a proton) at '*p*' *via* the electrical charge cloud formed by the molecule's electrons and nuclei is known as the Molecular Electrostatic Potential (MEP) at a specific position p(x,y,z) in the vicinity of a molecule. The ESP links a molecule's partial charge, dipole moment, electro-negativity, and chemical reactivity to its overall charge distribution. It leaves behind a visual way to comprehend a chemical structure's relative polarity. Additionally, it provides a useful quantity to describe the structure-activity relationship (SAR) for medicines and biomolecules, reactivity, and hydrogen bonding, among other things[26]. Distinct electrostatic potentials at the molecule's surface are represented by distinct colors. An area that is rich in electrons and could be the target of an electrophilic attack is represented by the color red. More electropositive domains, which could be the target of a nucleophilic assault, are shown by the color blue. Zero potential regions are shown by the green areas. The following formula is used to determine the molecular electrostatic potential values for the system under study[27].

$$V(r) = \sum \frac{Z_A}{|R_A - r|} - \int \frac{\rho(r')}{|r' - r|} dr \quad \ldots (1)$$

where, "the summation runs over all the nuclei A in the compound and polarization and reorganization effects are neglected. Z_A is the charge of the nucleus A, located at R_A, and ρ(r') is the electron density function of the molecule". Fig. 3 reports the MEP for the target molecule after it has been examined in the gaseous state in DMSO, THF, water, benzene, and ethanol solvents. Fig. 3 makes it evident that, for all liquids and gaseous phases, the blue color zone is produced over the hydrogen atoms of two hydroxyl groups, whereas the red color region is developed on the oxygen atom of the aldehyde group.

HOMO LUMO calculations

HOMO (Highest Occupied Molecular Orbital) and LUMO (Lowest Unoccupied Molecular Orbital) are

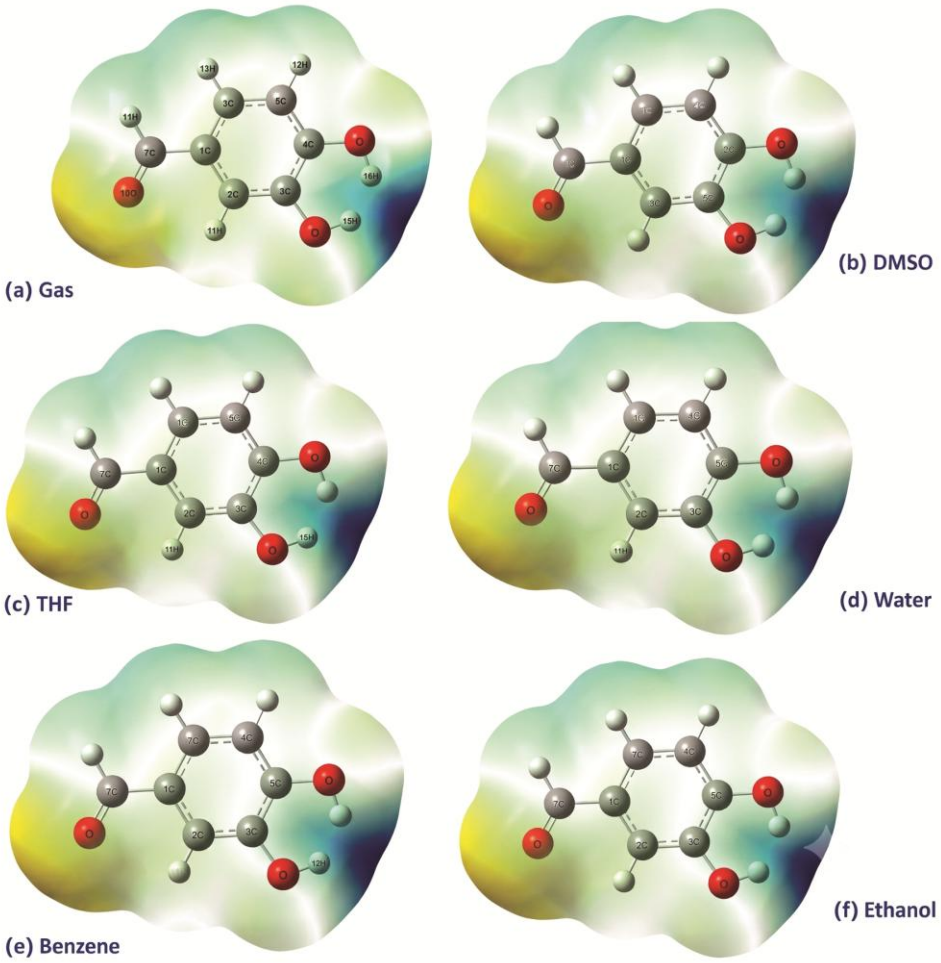

Fig. 3 — MEP diagram for PCA in (a) gaseous phase (b) DMSO (c) THF (d) Water (e) Benzene and (f) Ethanol solvents

the two primary variables in quantum chemistry computations. They are used to forecast the most reactive spots in electron systems and to characterize a variety of reactions in conjugated systems[28]. When electrons are transferred between donor and acceptor systems *via* a π conjugated route, the energy difference between the HOMO and LUMO is crucial. Furthermore, the stability of the molecule is influenced by two crucial orbitals: the lowest vacant molecular orbital and the highest occupied molecular orbital[29].

As seen in Fig. 4, the same basis set employed for the title molecule in the gaseous state-DMSO, THF, water, benzene, and ethanol solvents-is used to determine the molecule's HOMO and LUMO. Various calculations are done and reported in Table 4. In all cases, the HOMO is established on the whole molecule, whereas the LUMO is located except one hydroxyl group (-OH). The values in Table 4 clearly describe for the gaseous phase, that this is a stable molecule since its energy gap is found to be a larger one (4.7755 eV). Since the chemical hardness is greater than the chemical softness, this molecule can act as a hard molecule. A comparison chart is also created from the values in Table 4 and shown in Fig. 5. It is evident from Table 4 and Fig. 5 that all of the calculated values are nearly identical across all solvents.

Vibrational analysis

With 16 atoms, the molecule under research in the gaseous phase is capable of 42 normal modes of fundamental vibration. Thirteen of the 42 normal modes of vibration are out-of-plane, whereas 29 are in-plane. In-plane bands are symbolized by A′, whereas out-of-plane bands are marked by A″. Thus, the title molecule's 42 normal modes of vibration are dispersed as $\Gamma_{Vib} = 29\ A' + 13\ A''$. With each basic

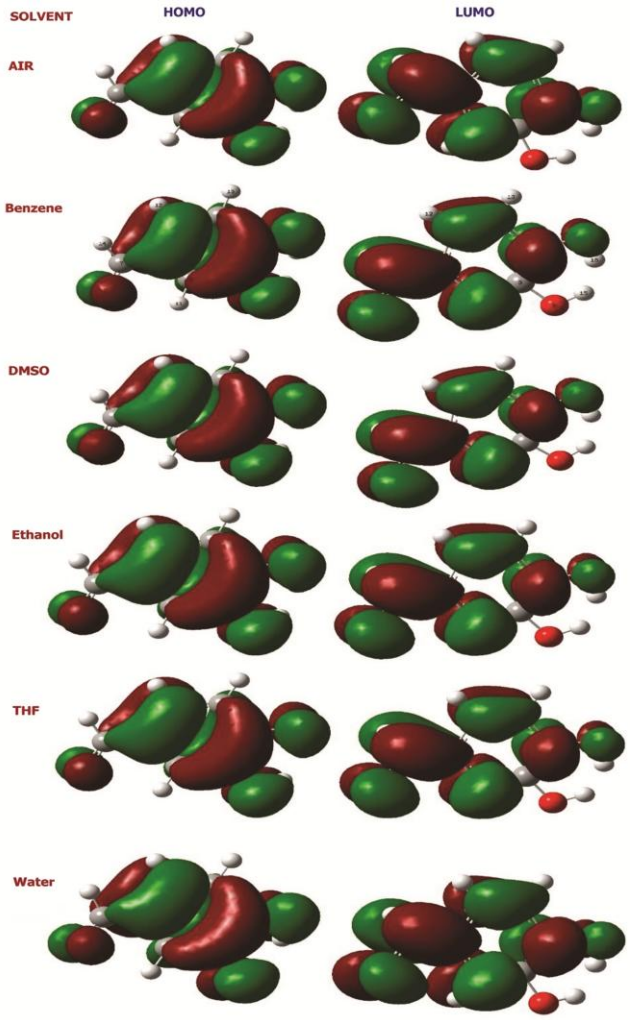

Fig. 4 — The HOMO and LUMO images of various solvents for the target molecule

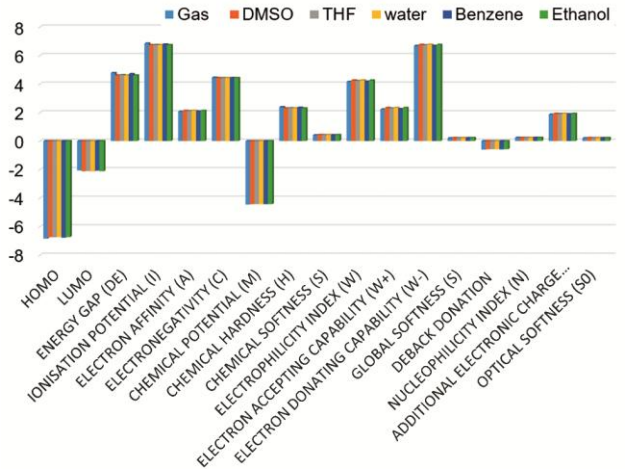

Fig. 5 — A comparison chart of HOMO - LUMO values and other calculated physical parameters for the target molecule in various solvents for PCA

wave number, all of the anticipated vibrational modes are numbered from lowest to biggest. The vibrational frequencies are theoretically determined using the DFT/6-311++G(d,p) basis set, and they are found to have good agreement when compared to the predicted DFT/6-31 G basis set data. The experimental IR data is also produced alongside the data in Table 5. The computed vibrational wave numbers are somewhat higher than the corresponding experimental data due to the combination of basis set imperfections and electron correlation effects (Fig. 6). It is discovered that the scaling factors are transferable to a variety of molecules and are simple to apply to the B3LYP level computations[31,32]. For the present study, the scaling factor used is 0.967. The VEDA 4 software is used to determine the potential energy distribution (PED). Together with the vibration assignment, the values are mentioned[33]. The distinctive spectral area, which is explained below, makes it simple to understand the title molecule's vibrational spectra.

OH vibrations

The hydroxyl (-OH) stretching vibrations are often seen in the 3500 cm^{-1} range[34,35]. Compared to a free -OH group vibration, the resultant peak is wider and more intense. This is because the two nearby -OH groups that are joined to the aromatic ring in the molecule form an intramolecular hydrogen bond. The –OH stretching frequencies in the B3LYP technique have been assigned calculated values of 3595 and 3532 cm^{-1}, whereas the empirically measured frequency is 3324 cm^{-1}. Between 1440 and 1260 cm^{-1}, the in-plane -OH deformation vibration manifests as a prominent band. However, it is moved to a lower wave number because to intramolecular hydrogen bonding. The in-plane bending vibrations of –OH for this molecule are produced at 1337, 1311, 1258, 1128, 1088, and 1050 cm^{-1}. In the 700–600 cm-1 range, a wide band is produced by the –OH out-plane bending vibrations. The –OH out-plane bending vibrations for this target molecule are found at 434, 419, 193, and 176 cm^{-1}. The calculated wave numbers accord well with both experimental and published data[36,37].

C=O stretching

The carbonyl (C=O) stretching vibrations in aldehydes are generated in the 1740–1720 cm^{-1} range[38,39]. But due to the presence of –OH groups in this molecule, the value is shifted to 1639 cm^{-1} in the theoretical spectrum, whereas the experimental signal is located at 1751 cm^{-1}.

Table 4 — The HOMO and LUMO values and other calculated physical parameters for the target molecule in various solvents

Sl. No	Parameter	Formula[30]	Charge (eV)					
			Gas	DMSO	THF	Water	Benzene	Ethanol
1	HOMO		–6.8436	–6.7348	–6.7457	–6.7321	–6.7785	–6.7348
2	LUMO		–2.0681	–2.1225	–2.1088	–2.1252	–2.0790	–2.1225
3	Energy gap (ΔE)		4.7755	4.6123	4.6369	4.6069	4.6995	4.6123
4	Ionisation potential (I)	$I = -E_{HOMO}$	6.8436	6.7348	6.7457	6.7321	6.7785	6.7348
5	Electron affinity (A)	$A = -E_{LUMO}$	2.0681	2.1225	2.1088	2.1252	2.079	2.1225
6	Electronegativity (χ)	$\chi = \frac{I + A}{2}$	4.4558	4.4286	4.4272	4.4286	4.4288	4.4286
7	Chemical potential (μ)	$\mu = -(\chi)$	–4.4558	–4.4286	–4.4272	–4.4286	–4.4288	–4.4286
8	Chemical hardness (η)	$\eta = \frac{I - A}{2}$	2.3878	2.3061	2.3185	2.3034	2.3498	2.3061
9	Chemical softness (S)	$S = \frac{1}{\eta}$	0.4188	0.4336	0.4313	0.4341	0.4256	0.4336
10	Electrophilicity index (ω)	$\omega = \frac{\mu^2}{2\eta}$	4.1574	4.2523	4.2269	4.2573	4.1736	4.2523
11	Electron accepting capability (ω^+)	$\omega^+ = \frac{(I + 3A)^2}{16(I - A)}$	2.2281	2.3263	2.3033	2.3309	2.2529	2.3263
12	Electron donating capability (ω^-)	$\omega^- = \frac{(3I + A)^2}{16(I - A)}$	6.6840	6.7549	6.7305	6.7596	6.6817	6.7549
13	Global softness (s)	$s = \frac{1}{2\eta}$	0.2094	0.2168	0.2157	0.2171	0.2128	0.2168
14	$\Delta E_{Back\ donation}$	$\Delta E = \frac{-\eta}{4}$	–0.5970	–0.5765	–0.5796	–0.5758	–0.5874	–0.5765
15	Nucleophilicity index (N)	$N = \frac{1}{\omega}$	0.2405	0.2352	0.2366	0.2349	0.2396	0.2352
16	Additional electronic charge (ΔN_{max})	$\Delta N_{max} = \frac{-\mu}{\eta}$	1.8661	1.9204	1.9095	1.9226	1.8848	1.9204
17	Optical softness (σ_0)	$\sigma_o = \frac{1}{\Delta E}$	0.2094	0.2168	0.2157	0.2171	0.2128	0.2168

Table 5 — Theoretical and experimental vibrational analysis for the target molecule with PED

S. No	S^y	Wavelength (cm^{-1})				Strength of signals	Assignment (PED)
		Experimental	6-31G	6-311++G(d,p)			
				Unscaled	Scaled		
1	A′		3706	3845	3595	s	νOH (100)
2	A′	3324	3611	3777	3532	s	νOH (100)
3	A′		3244	3199	2991	vw	νCH_{sym} (93)
4	A′	2874	3209	3171	2965	vw	νCH_{asym} (88)
5	A′	2824	3203	3169	2963	vw	νCH_{asym} (93)
6	A′	1875	2970	2892	2704	s	νCH_{χ} (99)
7	A′	1751	1700	1753	1639	vs	νCO (86)
8	A′	1650	1663	1643	1536	vs	νCC (29), νCC (18)
9	A′	1595	1653	1638	1532	w	νCC (34), νCC (20), δOH
10	A′	1535	1576	1551	1450	s	νCO (13), δCCH (16), δCCH (11), δCCH (13), δCCC (13) δOH

(*Contd.*)

Table 5 — Theoretical and experimental vibrational analysis for the target molecule with PED (*Contd*.)

S. No	S^y	Wavelength (cm^{-1})				Strength of signals	Assignment (PED)
		Experimental	6-31G	6-311++G(d,p)			
				Unscaled	Scaled		
11	A′	1444	1493	1479	1383	s	νCC (18), νCC (18), νCC (10), δOH
12	A′	1388	1457	1430	1337	m	νCC (13), δCOH (11), δOCH (42)
13	A′	1299	1426	1402	1311	m	δCOH (22), δOCH_{χ} (37)
14	A′		1379	1345	1258	w	νCC (22), δCOH (19)
15	A′	1192	13221	1305	1220	vs	νCC (18), νCO (34), δCCH (21)
16	A′	1167	1295	1280	1197	w	νCO (15), δCCH (26), δCCH (10)
17	A′	1118	1221	1206	1128	s	νCC (19), δCOH (35), δCCH (11)
18	A′		1194	1167	1091	m	νCC (15), νCC (20),νCO (14), δCCH (11), δCCH (24)
19	A′		1171	1163	1088	vs	δCOH (39), δCCH (22)
20	A′	975	1129	1123	1050	m	νCO (11), δCOH (12), δCCH (22)
21	A″	946	1036	1019	953	vw	γCCCH (54), γCCCO (31)
22	A′	876	993	982	918	vw	νCC (17), νCC (10), νCO (12), δCCC (12)
23	A″	813	979	947	886	vw	γCCCH (45), γCCCH (37)
24	A″	775	917	881	824	m	γCCCH (68), γCCCC (10)
25	A″	754	855	827	773	m	γCCH (38), γCCCH (45)
26	A′		815	810	757	vw	νCO (17), δCCC (13), δCCC (27)
27	A′		770	761	712	s	νCO (17), νCO (12),δCCC (12), δCCO (11), δCCC (27)
28	A″	630	727	701	655	vw	γCCCH (10), γCCCO (34), γCCCO (30)
29	A′	590	637	635	594	m	νCC (13), δCCC (12) δCCO (26), δCCO (13)
30	A″		606	587	549	vw	γCCCC (20), γCCCC (14), γCCCC (11), γCCCO (16), γCCCC (12)
31	A′		579	575	538	vw	δCCO (13), δCCC (15), δCCC (12), δCCO (13), δCCO (22)
32	A′	449	535	493	461	vw	νCC (11), νCC (10), δCCC (17), δCCO (14), δCCO (19)
33	A″		495	464	434	m	γCCOH (77)
34	A″		468	448	419	m	γCCOH (17), γCCCH (12), γCCCC (14), γCCCO (16), γCCCO (16)
35	A′		395	390	365	vw	νCC (10), νCC (16), δCCC (15), δCCO (13)
36	A″		383	372	348	vw	γCCCH (14), γCCCC (14), γCCCO (24), γCCCO (12), γCCCO (21)
37	A′		321	313	293	vw	δCCC (17), δCCO (32), δCCO (35)
38	A″		306	213	199	vw	γCCCC (30), γCCCC (15), γCCCC (16), γCCCO (12), γCCCO (19)
39	A″		224	206	193	m	γCCOH (47), γCCCO (19)
40	A″		210	188	176	s	γCCOH (49), γCCCO (14), γCCCC (12)
41	A′		187	184	172	w	δCCC (62), δCCO_{χ} (20)
42	A″		105	97	91	vw	γCCCO (19), γCCCC (34), γCCCO (31)

"Sy, Symmetry; s, strong; vs, very strong; w, weak; vw, very weak; m, medium; ν, stretching; sym, symmetric; asym, asymmetric; γ, out plane bending; δ, in plane bending; χ, CHO group"

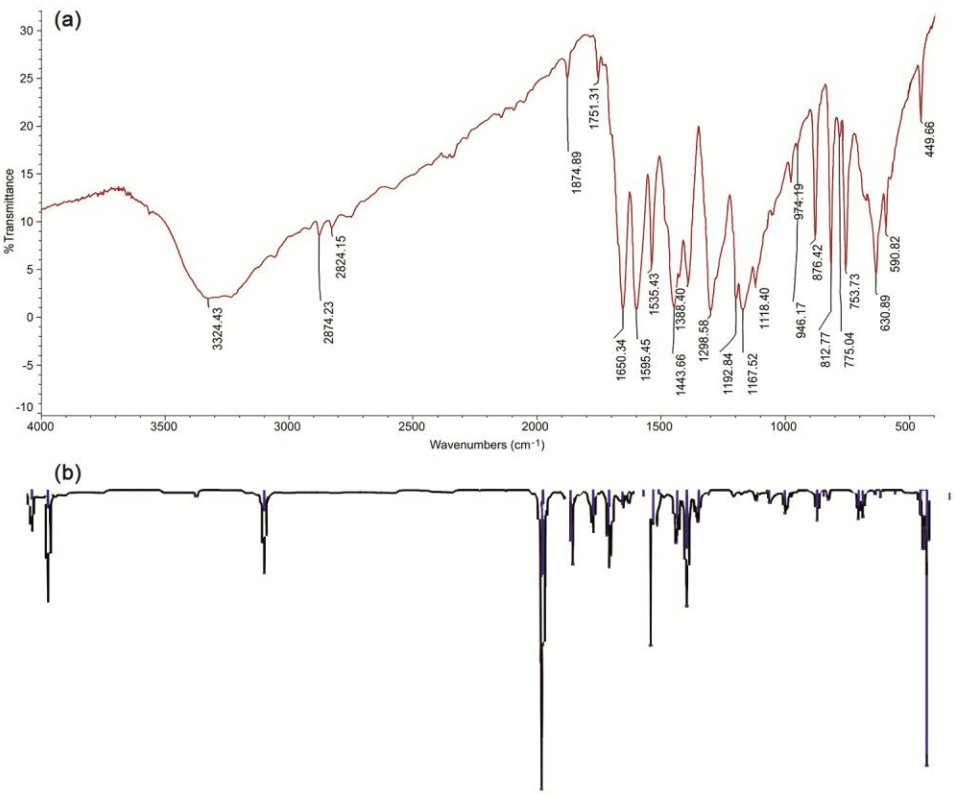

Fig. 6 — (A) Experimental (B) Theoretical IR spectra of title compound

The C-O stretching mode of vibrations contributes significantly to the signals at 964-890 cm^{-1}. These peaks are found at 1450, 1220, 1197, 1091, 1050, 918, 757, and 712 cm^{-1} for the given molecule. While the out-plane bending vibrations are formed at 655, 549, 419, 348, 199, 193, 176, and 91 cm^{-1}, the C-O in-plane bending vibrations are found at 712, 594, 538, 461, and 365 cm^{-1}.

C-C vibrations

The 1625–1430 cm^{-1} range is where the aromatic C–C stretching vibrations are found[24]. For this study, this variety of peaks is observed at 1536, 1532, 1383, 1337, 1258, 1220, 1128, 1091, 918, 594, 461, and 365 cm^{-1} as a mixture of strong, very strong, medium, and very weak peaks. The CCC in-plane bending vibrations are located at 1450, 918, 757, 712, 594, 538, 461, 365, 293, and 172 cm^{-1} whereas the CCC out-of-plane bending vibrations are located at 824, 594, 419, 199, 176, and 91 cm^{-1} respectively. Wave numbers can be altered by slight variations in force constants or decreased mass ratios, which are mostly caused by the degree of mixing between the ring and the replacement group.

CH vibrations

Since 3,4-dihydroxybenzaldehyde is a tri-substituted benzene molecule, it has only three CH moieties. So they can develop C-H stretching vibrations (symmetric and asymmetric). The CH asymmetric stretching vibrations are detected at 2965 and 2963 cm^{-1}, but the CH stretching vibration is found at 2991 cm^{-1} as a very faint signal[24]. The areas of 1300–1000 cm^{-1} and 600–1000 cm^{-1}, respectively, are where the in-plane and out-of-plane CH vibrations are seen. For the present study, CH in-plane bending vibrations are located at 1450, 1220, 1197, 1128, 1091, 1088, and 1050 cm^{-1}. The peaks seen at 953, 886, 824, 773, 701, 419, and 348 cm^{-1} are responsible for CH out-plane bending vibrations. They show good agreement with experimental values.

Aldehyde group CHO stretching vibrations often occur in the 2871–2806 cm^{-1} range[40]. The C-H stretching vibration, which is calculated in this study at 2704 cm^{-1} as a strong peak, agrees well with the reported value. The in-plane bending vibrations show up as medium bands at 1337 and 1311 cm^{-1}, respectively. It is possible to attribute a medium band that appears at 594 cm^{-1} to C=O in-plane bending

vibrations. Also, very weak signals at 293, and 172 cm^{-1} peaks are also responsible for aldehyde in-plane bending vibrations.

UV-Vis spectral analysis

To understand the specifics of the experimental (ethanol) and theoretical (benzene, DMSO, ethanol, THF, and water solvents) spectra, the electronic transition of the molecule being studied is computed using the TDDFT/B3LYP/6-311++G(d,p) basis set and is displayed in Fig. 7.

The GaussSum 03 tool is used to calculate the wavelength (nm), energy (cm^{-1}) and oscillator strength (f) which are given along with the major and minor contributions in Table 6. The theoretical spectrum (ethanol) predicts that one intense peak is observed at 268.44 nm. The molar absorption coefficient for this absorption band (ε) is observed as 37251.52 cm^{-1} which arises due to the major contribution of HOMO-1→LUMO (76%), and HOMO→LUMO (16%) and the minor contribution from HOMO→LUMO+2 (7%). The signal developed at 297.95 nm with a molar absorption coefficient (ε) of 33562.34 cm^{-1} arises due to the major electronic transitions from HOMO→LUMO (80%), HOMO-1→LUMO (14%), as well as the minor contributions from HOMO-1→LUMO+2 (4%), and HOMO→LUMO+2 (2%). Similarly, HOMO-2→LUMO (97%) contributes in a larger amount, with an energy of 31024.11 cm^{-1} to produce a signal at 322.32 nm. The oscillator strengths measured for the three transitions are found to be 0.2158, 0.1641 and 0.0001 respectively. The UV spectrum with other solvents is shown in Fig. 7.

Natural Bond Orbital analysis

Since all orbital features are mathematically selected to include the greatest percentage of the molecule's electron density, Natural Bond Orbital (NBO) analysis offers the most accurate "natural Lewis structure" representation of ϕ. Furthermore, the NBO method offers information on interactions in both virtual and filled orbital regions, which may be useful for analyzing interactions between and inside molecules.

The NBO inquiry examines the relationships between donors and acceptors using the second-order Fock matrix[41]. The interaction causes a loss of occupancy from the localized NBO of the idealized Lewis structure into an empty non-Lewis orbital of a molecule. The stabilisation energy E(2) connected to the delocalization i→j is evaluated for each donor (i) and acceptor (j)

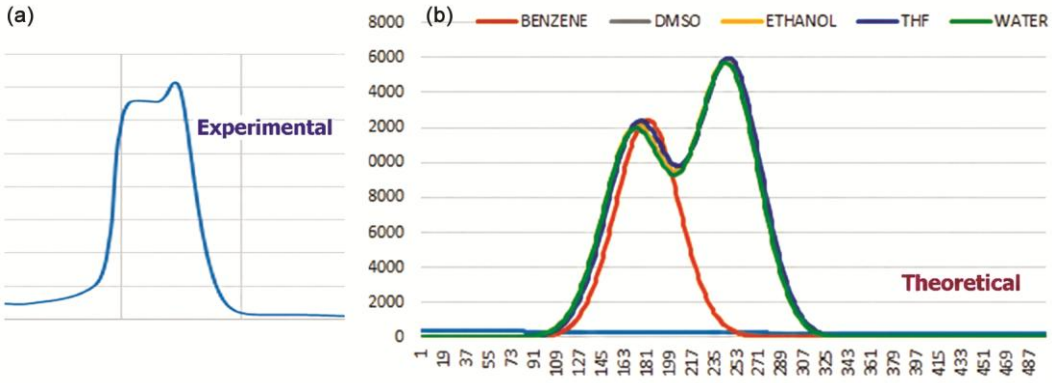

Fig. 7 — UV - Experimental (A) spectrum in ethanol and Theoretical (B) spectrum in benzene, DMSO, ethanol, THF and water for the molecule of interest

Table 6 — The UV-Vis wavelength, energy, oscillator strength with major and minor contributions for the title molecule

Wavelength (nm)		Energy (cm^{-1})	Osc. Strength (f)	Major contributions*	Minor contributions
Experimental (Ethanol solvent)	Calculated				
344	322.32	31024.11	0.0001	HOMO-2→LUMO (97%)	–
313	297.95	33562.34	0.1641	HOMO→LUMO (80%) HOMO-1 →LUMO (14%),	HOMO-1→LUMO+2 (4%), HOMO→LUMO+2 (2%)
–	268.44	37251.52	0.2158	HOMO-1→LUMO (76%), HOMO→LUMO (16%)	HOMO→LUMO+2 (7%)

* → (HOMO is located at MO 36)

$$E_2 = \Delta E_{i,j} = q_i \frac{F(i,j)^2}{\varepsilon_j - \varepsilon_i} \quad \ldots (2)$$

"where q_i is the donor orbital occupancy, ε_i and ε_j are diagonal elements, and F(i,j) is the off-diagonal NBO Fock matrix element".

The NBO analysis is a useful technique for investigating intra- and intermolecular bonding as well as interactions between the bonds. Additionally, it provides a solid basis for studying charge transfer (CT) or conjugative interactions in molecular systems. James *et al*. and J. N. Lu *et al*. disclose certain donor and acceptor orbitals and the interaction stabilization energy that came from the second-order micro-disturbance theory[42,43]. The stronger the contact between electron donors and acceptors, the higher the E(2) value[44]. A stabilizing donor-acceptor interaction is associated with the delocalization of electrons from vacant non-Lewis orbitals (anti-bond or Rydberg) and occupied Lewis-type (bond or lone pair) NBO orbitals.

The DFT/B3LYP/6-311++G(d,p) basis set serves for NBO analysis of the title molecule with the aim to clarify intramolecular elucidation and the delocalization of electron density inside the molecule. The intramolecular interactions are done by the orbital overlap between σ(C–C) and σ*(C–C) and π(C–C) and π*(C–C) bond orbitals. It results in intramolecular charge transfer (ICT), and they are the reasons for the stabilization of the molecular system. The electron density of conjugated bonds in the aromatic ring (~1.9 e) validates strong delocalization clearly.

In this molecule, σ → σ*, π → π*, LP → σ*, LP → π*, and π* → π* interactions are reported selectively in Table 7. The interactions of σ(C1-C2) → σ*(C3-O8), σ(O9-H16) → σ*(C4-O6), and σ(C2-H11) → σ*(C1-C5) are responsible for the stabilisation with energies of 4.87, 4.72, 4.67 kcal/mol, respectively. The interactions of π(C2-C3) → π*(C4-C6), π(C1-C5) → π*(C2-C3), and π(C1-C5) → π*(C7-O10) stabilizes the molecule with energies of 22.51, 20.78 and 20.73 kcal/mol, respectively. 21.44 and 16.43 kcal/mol energies are due to LP(2) of O10 to σ*(C7-H14) and σ*(C1-C7) respectively, which are useful to stabilise the molecule. The π*(C7-O10) → π*(C1-C5) and π*(C4-C6) → π*(C1-C5) are greatly helpful to stabilise the molecule with energies of 148.00 and 271.94 kcal/mol, respectively. LP(2) O9 → π*(C4-C6) and LP(2) O8 → π*(C2-C3) interactions with energies of 25.84 and 24.64 kcal/mol respectively further stabilise the molecule. Intramolecular hydrogen bonding is observed within the molecule. The interaction between σ(O9-H16) to σ*(O8-H15) and σ(O8-H15) to σ*(O9-H16) with energies of 3.33 and 3.85 kcal/mol is also responsible for the stability of the molecule.

Study of weak interactions

The investigation of the weak interaction of a molecule is determined by Multiwfn 3.8 software. The hypothesis of "Atoms in a Molecule" (AIM) is helpful in explaining the weak interactions within molecules. The non-covalent interaction is calculated using the Reduced Density Gradient (RDG) iso-surface function, which is defined as,

$$RDG(r) = \frac{1}{2(3\pi^2)^{1/3}} \frac{|\nabla\rho(r)|}{\rho(r)^{4/3}} \quad \ldots (3)$$

The Reduced Density Gradient is plotted against the sign of λ_2 along the density ρ to get the NCI plot. The plot specifies spikes in the low-density gradient region. It is a classic trace of NCI interaction that is stronger and stronger when it moves away from zero[45].

The NCI plot of RDG and isosurface function is shown in Fig. 8. From Fig. 8a, it is evident that the spikes around -0.040 a.u. mean the presence of a hydrogen bond, and the spikes developed between -0.020 and +0.0010 a.u. are due to the presence of weak van der Waals attraction. The spikes above +0.020 a.u. represent the presence of the steric effect. Two cube files (.cub) are generated and viewed by VMD 1.9.4 software. The picturized (Fig. 8b) isosurface shows that the red color sphere inside the ring is accountable for the steric effect. The greenish-red-like circles are mentioning the presence of van der Waals force of attraction in the molecule. They appear in the caves near –CHO, CH, as well as OH-OH groups respectively. The dark blue color sphere between the two hydroxy groups represents the presence of intra molecular hydrogen bonding.

Shaded surface map with a projection of LOL analysis

The Multiwfn 3.8 tool is a program that helps us understand the shaded surface map with a projection

Table 7 — Analysis of the Fock matrix in the NBO basis for the title molecule using second order perturbation theory

Sl. No	Type	Donor NBO (i)	ED/e	Type	Acceptor NBO (j)	ED/e	E(2)	E(j)-E(i)	F(i,j)
1	σ	C1-C2	1.9692	σ*	C1-C5	0.0217	3.87	1.26	0.063
2	σ	C1-C2	1.9692	σ*	C3-O8	0.0239	4.87	1.03	0.063
3	σ	C1-C5	1.9759	σ*	C1-C2	0.0216	3.82	1.27	0.062
4	σ	C1-C5	1.9759	σ*	C1-C7	0.0556	1.38	1.16	0.036
5	π	C1-C5	1.6462	π*	C2-C3	0.3472	20.78	0.27	0.067
6	π	C1-C5	1.6462	π*	C4-C6	0.3859	18.86	0.27	0.064
7	π	C1-C5	1.6462	π*	C7-O10	0.1220	20.73	0.27	0.071
8	σ	C2-C3	1.9726	σ*	C3-C4	0.0392	4.36	1.26	0.066
9	σ	C2-C3	1.9726	σ*	C4-O9	0.0231	3.39	1.05	0.053
10	π	C2-C3	1.6704	π*	C1-C5	0.3994	18.26	0.30	0.067
11	π	C2-C3	1.6704	π*	C4-C6	0.3859	22.51	0.28	0.072
12	σ	C2-H11	1.6704	σ*	C1-C5	0.0217	4.67	1.09	0.064
13	σ	C2-H11	1.6704	σ*	C3-C4	0.0392	3.86	1.06	0.057
14	σ	C3-C4	1.9752	σ*	C2-C3	0.0203	4.44	1.30	0.068
15	σ	C3-C4	1.9752	σ*	C4-C6	0.0223	4.50	1.29	0.068
16	σ	C4-C6	1.9728	σ*	C3-C4	0.0392	4.26	1.26	0.066
17	σ	C4-C6	1.9728	σ*	C3-O8	0.0239	3.06	1.05	0.051
18	π	C4-C6	1.6546	π*	C1-C5	0.3994	20.42	0.30	0.071
19	π	C4-C6	1.6546	π*	C2-C3	0.3472	19.19	0.29	0.067
20	σ	C5-C6	1.9754	σ*	C1-C7	0.0556	3.19	1.16	0.055
21	σ	C5-C6	1.9754	σ*	C4-O9	0.0231	4.26	1.03	0.059
22	σ	C5-H12	1.9796	σ*	C1-C2	0.0216	4.57	1.10	0.063
23	σ	C5-H12	1.9796	σ*	C4-C6	0.0223	3.13	1.08	0.052
24	σ	C6-H13	1.9788	σ*	C1-C5	0.0217	3.27	1.09	0.053
25	σ	C6-H13	1.9788	σ*	C3-C4	0.0392	3.92	1.07	0.058
26	σ	C7-O10	1.9961	σ*	C1-C5	0.0217	1.46	1.61	0.043
27	π	C7-O10	1.9794	π*	C1-C5	0.3994	5.22	0.39	0.045
28	σ	C7-H14	1.9874	σ*	C1-C2	0.0216	3.79	1.11	0.058
29	σ	O8-H15	1.9752	σ*	C2-C3	0.0203	4.49	1.32	0.069
30	σ	O8-H15	1.9752	σ*	O9-H16	0.0260	3.85	1.12	0.059
31	σ	O9-H16	1.9765	σ*	C4-C6	0.0223	4.72	1.31	0.070
32	σ	O9-H16	1.9765	σ*	O8-H15	0.0230	3.33	1.13	0.055
33	LP(1)	O8	1.9731	σ*	C3-C4	0.0392	4.27	1.18	0.064
34	LP(2)	O8	1.8894	π*	C2-C3	0.3472	24.64	0.37	0.090
35	LP(1)	O9	1.9747	σ*	C3-C4	0.0392	4.41	1.20	0.065
36	LP(2)	O9	1.8774	π*	C4-C6	0.3859	25.84	0.36	0.093
37	LP(2)	O10	1.8866	σ*	C1-C7	0.0556	16.43	0.72	0.098
38	LP(2)	O10	1.8866	σ*	C7-H14	0.0612	21.44	0.63	0.105
39	π*	C4-C6	0.3859	π*	C1-C5	0.3994	271.94	0.01	0.082
40	π*	C7-O10	0.1220	π*	C1-C5	0.3994	148.00	0.01	0.070

"E(2) is the energy of hyper conjugative interaction (stabilization energy)
E(j)-E(i) is the energy difference between donor and acceptor i and j NBO orbitals
F(i,j) is the Fock matrix element between i and j NBO orbitals
ED/e is the electron density of donor and acceptor NBO orbitals
LP(n)A is a valence lone pair orbital (n) on A atom"

of LOL. It explores the electron depletion area and the electron-rich area[46] Localised Orbital Locator (LOL), according to Schmider and Becke, is a function that is used to find localised high localisation zones[47]. It is defined as:

$$\mathrm{LOL}(r) = \frac{\tau(r)}{1+\tau(r)} \qquad \ldots (4)$$

"where $\tau(r)$ (dimensionless variable) is $g_0(r) / g_{(r)}$". It is always determined by the kinetic energy of one positive electron. It is described as,

$$g(r) = \frac{1}{2}\sum \nabla_{\Psi_i}(r)\nabla\psi_i(r) \qquad \ldots (5)$$

"where Ψ_I (r) is the Hatree–Fock or the Kohn-Sham orbital".

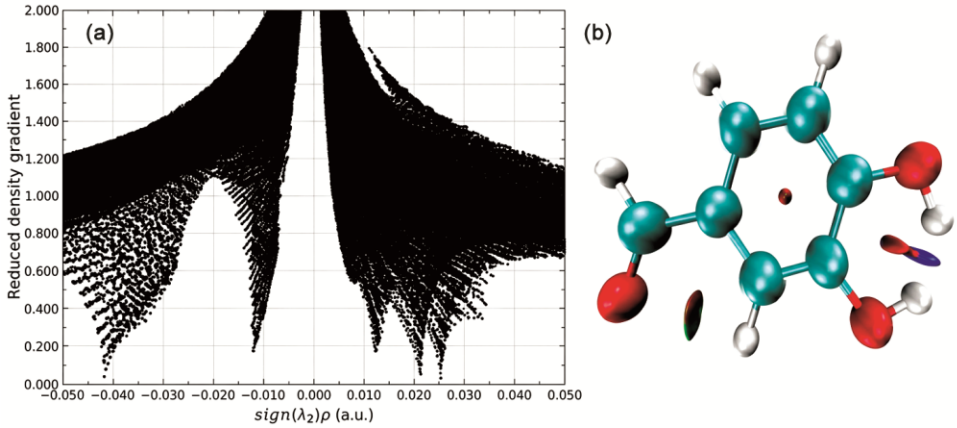

Fig. 8 — (a) The NCI analysis (b) isosurface function for the target molecule

In a specific domain of a molecule, the larger the LOL, the more likely it is that the electron motion is controlled within it. Fig. 9 displays the evaluation of the shaded surface map with a projection of the localised orbital locator (LOL) for the chemical under inquiry. In this, the blue coloured rings surrounding the nucleus denote the high electron depletion zones between the valence shell and inner shell. Each carbon atom in the aromatic ring has a region where electrons are less abundant. The highly localised electron zones are represented by the colour red. The molecule is stabilized by the electrons' propensity to be concentrated on its outer edge.

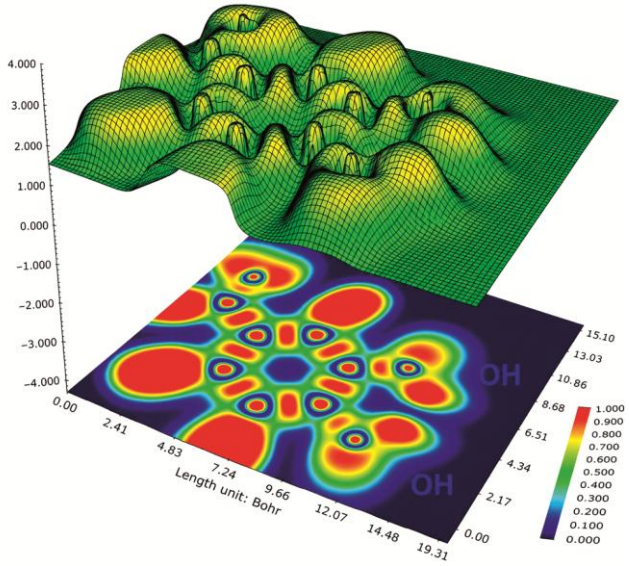

Fig. 9 — Shaded surface map with a projection of LOL analysis of the target molecule (Here the Z-axis is LOL)

Fukui function analysis

Reactivity indices are all that Fukui functions (FF) are. They make assumptions about which atoms in a molecule are capable of gaining or losing an electron. They are otherwise called cites of nucleophilic attacks or electrophilic attacks. It is defined[48] as,

$$f(r)=\left(\frac{\delta\rho(r)}{\delta(N)}\right)r \qquad \ldots (6)$$

"where '$\delta\rho$' is the electronic density, 'N' is the number of electrons, and 'r' is the external potential exerted by the nucleus". In order to represent chemical selectivity and reactivity, the Fukui function is a crucial tool for local density functional descriptors. It states that altering the amount of electrons in a chemical species will cause it to change its density. Consequently, it provides a useful indication of the electron density's tendency to function at a certain location while absorbing or donating electrons[49,50]. The definition for the corresponding condensed or atomic Fukui function on the fth atom site is:

$$f_j^{+}=q_j(N+1)-q_j(N) \text{ (for nucleophilic attack)} \qquad \ldots (7)$$

$$f_j^{-}=q_j(N)-q_j(N-1) \text{ (for electrophilic attack)} \qquad \ldots (8)$$

$$f_j^{0}=\frac{1}{2}\left[q_j(N+1)-q_j(N-1)\right] \text{ (for radical attack)} \qquad \ldots (9)$$

"where, f_j^{+}, f_j^{-}, f_j^{0} are nulcleophilic, electrophilic and free radicals, respectively. Here 'q_j' is the atomic

charge (assessed from Mulliken population analysis and electrostatic derived charges, *etc*.) and j^{th} atomic sites is the neutral (N), anionic (N+1), or cationic (N-1) chemical species".

A dual descriptor, [f(r)], has been developed by Morrel *et al*. Its definition is the difference between the nucleophilic and electrophilic Fukui functions, and it is represented by[51],

$$\Delta f(r) = \left[f^{+}(r) - f^{-}(r) \right] \quad \ldots (10)$$

"If $\Delta f(r) > 0$, then it is more prone to nucleophilic attack, and if $\Delta f(r) < 0$, then it is a favourable site for electrophilic attack". From the sign of the values, we can understand the type of attack. A positive value means the choice of nucleophilic attack, and a negative value indicates the choice of electrophilic attack.

The MPA and NPA values for the target molecule are analysed and reported in Table 8, along with $\Delta f(r)$ values. According to the MPA analysis, for cations and anions, the possible attack is a nucleophilic attack, since the maximum observed value is 0.3177 a.u. (1C) and 0.3311 a.u. (2C), respectively. For a neutral molecule, the electrophilic attack is possible at 5C since the value is -1.6784 a.u. The reactivity order for nucleophilic attack for cations and anions is 1C > 3C > 4C > 9O > 10O and 2C > 7C > 4C > 10O > 5C respectively. The order of electrophilic attack for a neutral molecule is 5C > 4C > 8O > 10O > 9O.

For NPA analysis, for cations, neutral and anions, only electrophilic attack is possible at 8O (-0.5566 a.u.), 8O (-0.6494 a.u.), and 9O (-0.7295 a.u.), respectively. The order for cations is 8O > 9O > 10O > 2C > 6C; for neutral it is 8O > 9O > 10O > 5C > 2C; and for anions, it is 9O > 8O > 10O > 5C > 6C, respectively. From Table 8, for NPA analysis, the values predict that all the atoms are prone to nucleophilic attack only since $\Delta f(r) > 0$. The behaviour of a molecule as an electrophilic and nucleophilic attack depends on the local behaviour of molecule during the reaction.

NHO directional analysis

Using the same basis set, a Natural Hybrid Analysis (NHO) analysis is conducted for the current molecule. The angular characteristics of the natural hybrid orbitals are summarized in Table 9. The "direction" of a sp^{λ} hybrid is specified by the polar (θ) and azimuthal (φ) angles of the vector defining the p-component of the hybrid (in the ESS coordinate system). The hybrid direction is found numerically to correspond to the greatest angular amplitude for more general $sp^{\lambda}d^{\mu}$ hybrids. The computer calculates the bending of the bond, which is represented as the deviation angle ("Dev," in degrees), between the hybrid direction and the direction of the line of centers between the two nuclei[52].

For example, the $\sigma_{C1\text{-}C7}$ bond (NBO 4) is bent away from the line of C-C centers by 2.1° in hybrid 2 and it is aligned well in Hybrid 1. LP(1) and LP(2) of O8, O9, and O10 are not at all deviated from their natural geometrical alignment in their Hybrid models 1 and 2. The $\sigma_{C2\text{-}C3}$ (NBO 5)bond angle is slightly deviated for

Table 8 — Fukui function analysis according to MPA and NPA values for the title molecule

S. No	Atoms	MPA (a.u.)			NPA (a.u.)			
		Cation	Neutral	Anion	Cation	Neutral	Anion	Δf(r)
1	1C	0.3177	1.4548	0.0187	0.1806	0.0151	0.0291	0.1515
2	2C	–0.1511	–0.0845	0.3311	–0.2877	–0.2692	–0.3133	0.0256
3	3C	0.2359	0.0101	–0.1104	0.3082	0.2204	0.1370	0.1712
4	4C	0.2140	–0.6943	0.2481	0.4610	0.4047	0.4503	0.0107
5	5C	0.0511	–1.6784	0.0870	–0.1772	–0.3033	–0.3756	0.1984
6	6C	–0.0093	0.6379	–0.0194	–0.2106	–0.2381	–0.3498	0.1392
7	7C	–0.0670	–0.0701	0.2748	0.4047	0.4563	0.2565	0.1482
8	8O	0.1142	–0.3016	0.0001	–0.5566	–0.6494	–0.6858	0.1292
9	9O	0.1880	–0.2259	0.0232	–0.4451	–0.6093	–0.7295	0.2844
10	10O	0.1179	–0.2602	0.2017	–0.3475	–0.4925	–0.6612	0.3137
11	11H	0.0029	0.1601	–0.0243	0.1928	0.1680	0.1150	0.0778
12	12H	–0.0061	0.1323	–0.0063	0.2027	0.1775	0.1355	0.0672
13	13H	–0.0021	0.2138	0.0003	0.2320	0.1946	0.1603	0.0717
14	14H	0.0019	0.1300	–0.0236	0.0399	–0.0111	–0.0584	0.0983
15	15H	–0.0033	0.2870	–0.0003	0.5137	0.4689	0.4423	0.0714
16	16H	–0.0047	0.2890	–0.0008	0.4891	0.4672	0.4477	0.0414

Table 9 — NHO directionality and bond bending nature of the title molecule under investigation

NBO	Bond type	Atom pair	Line of centers		Hybrid 1			Hybrid 2		
			Theta	Phi	Theta	Phi	Deviation	Theta	Phi	Deviation
3	π	C1-C5	90.0	63.4	0.0	0.0	90.0	180.0	0.0	90.0
4.	σ	C1-C7	90.0	182.7	–	–	–	90.0	0.6	2.1
5.	σ	C2-C3	90.0	3.8	–	–	–	90.0	185.8	2.0
6.	π	C2-C3	90.0	3.8	0.0	0.0	90.0	180.0	0.0	90.0
7.	σ	C2-H11	90.0	242.4	90.0	243.8	1.4	–	–	–
8.	σ	C3-C4	90.0	63.4	90.0	60.6	2.8	90.0	246.8	3.4
9.	σ	C3-O8	90.0	305.7	90.0	307.1	1.5	–	–	–
10.	σ	C4-C6	90.0	122.3	90.0	121.3	1.0	–	–	–
11.	π	C4-C6	90.0	122.3	179.9	128.1	90.0	0.0	0.0	90.0
12.	σ	C4-O9	90.0	3.3	90.0	0.9	2.4	90.0	181.9	1.3
13.	σ	C5-C6	90.0	3.1	90.0	1.8	1.3	–	–	–
14.	σ	C5-H12	90.0	122.3	90.0	123.6	1.2	–	–	–
16.	σ	C7-O10	90.0	240.8	–	–	–	90.0	61.9	1.1
17.	π	C7-O10	90.0	240.8	180.0	0.0	90.0	0.0	0.0	90.0
18.	σ	C7-H14	89.9	119.4	90.0	121.9	2.5	–	–	–
19.	σ	O8-H15	88.6	17.5	88.5	16.4	1.1	–	–	–
20.	σ	O9-H16	90.0	287.9	89.9	290.9	3.0	–	–	–
31.	LP(1)	O8	–	–	90.6	257.8	–	–	–	–
32.	LP(2)	O8	–	–	178.7	27.2	–	–	–	–
33.	LP(1)	O9	–	–	89.8	49.6	–	–	–	–
34.	LP(2)	O9	–	–	179.9	35.2	–	–	–	–
35.	LP(1)	O10	–	–	90.0	238.5	–	–	–	–
36.	LP(2)	O10	–	–	90.0	330.6	–	–	–	–
245	π*	C1-C5	90.0	63.4	0.0	0.0	90.0	180.0	0.0	90.0
248	π*	C2-C3	90.0	3.8	0.0	0.0	90.0	180.0	0.0	90.0
253	π*	C4-C6	90.0	122.3	179.9	128.1	90.0	0.0	0.0	90.0
259	π*	C7-O10	90.0	240.8	180.0	0.0	90.0	0.0	0.0	90.0

hybrid 2 by the factor of 2.0° and in the case of $\pi_{C2\text{-}C3}$, it is deviated by a very large factor of 90° for hybrid models 1 and 2. From the above discussions, we can conclude that the slight changes in geometrical parameters occurred due to the optimisation of the title molecule.

Hole-electron excitation analysis

The Multiwfn 3.8 is a very gigantic program to complete electron excitation analysis theoretically. Additionally, it implies a profound understanding of every kind of electron transfer feature found in a molecule. It is a very practical way to disclose the nature of the electron excitations[53]. The molecule under investigation has two –OH groups (electron donors) attached to the benzene moiety (a bridge or π-linker) and an electron-withdrawing group (-CHO). such that electrons can go *via* the bridge from the electron donors to the acceptors with ease. Hence, it is decided to investigate the electron excitation properties of this title molecule.

The molecule is first optimized by the same basis set initially. Then the TD-DFT calculation is carried out with the CAM-B3LYP basis set using the usual IO*p*(9/40=4) keyword. The ten lowest singlet excited states are recorded theoretically. The achieved Sm index, Sr index, D index, H index, τ index, excitation energy, Coulomb attractive energy, Δr, and Λ (Lambda) values are analysed at the same level of theory and shown in Table 10. The obtained hole electron distribution, $c_{hole} - c_{elec}$ function, Sr function, and Charge Density Difference (CDD) for the molecule of interest are summarized and shown in Fig. 10. The large D index values are observed at S0 → S4 (2.122 Å), S0 → S9 (2.303 Å), and S0 → S10 (3.033 Å) excitations and can obviously be considered charge transfer (CT) excitations. For these three excitations, Fig. 10 also shows that there is a significant gap between the centers of the green (electron) and blue (hole) isosurfaces (centreoids of c_{hole}–c_{elec}).

According to the earlier reports[30], if the Sr index value is greater than 0.8 a.u. it means it can follow the

Table 10 — Hole-electron interaction properties for the target molecule

Excited state	Sm (a.u)	Sr (a.u)	D index (Å)	H index (Å)	τ index (Å)	Excitation energy (eV)	Coulomb attractive Energy (eV)	Δr	Λ (Å)
S1	0.2423	0.4815	1.017	1.679	–0.206	3.964	8.1253	0.4216	1.9380
S2	0.5046	0.7987	0.993	2.219	–0.705	4.663	6.4271	0.6577	1.3951
S3	0.5349	0.8199	1.087	2.205	–0.705	5.047	6.4773	0.6243	1.2743
S4	0.1381	0.3397	2.122	2.463	0.711	5.526	4.6728	0.2312	2.9795
S5	0.5641	0.8280	1.039	2.238	–0.590	5.979	6.2654	0.6259	0.8268
S6	0.1304	0.3321	0.942	3.013	–0.996	6.279	4.3338	0.1962	2.8751
S7	0.1200	0.3119	1.082	3.151	–0.909	6.413	4.0999	0.1793	2.9508
S8	0.5891	0.8375	0.454	2.180	–0.952	6.574	6.4597	0.7331	0.6347
S9	0.1144	0.3005	2.303	2.819	0.596	6.596	4.1722	0.2092	2.2561
S10	0.0658	0.2147	3.033	1.836	1.861	6.829	4.7357	0.2042	3.1528

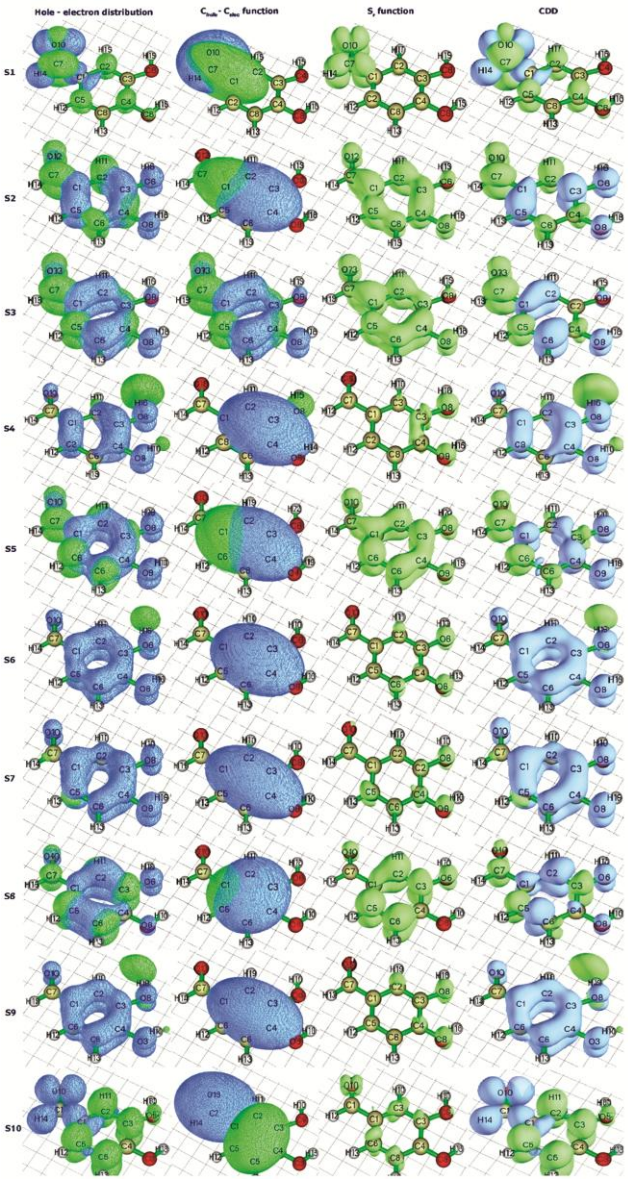

Fig. 10 — The hole electron distribution, $c_{hole} - c_{elec}$ function, Sr function and Charge Density Difference (CDD) for the target molecule

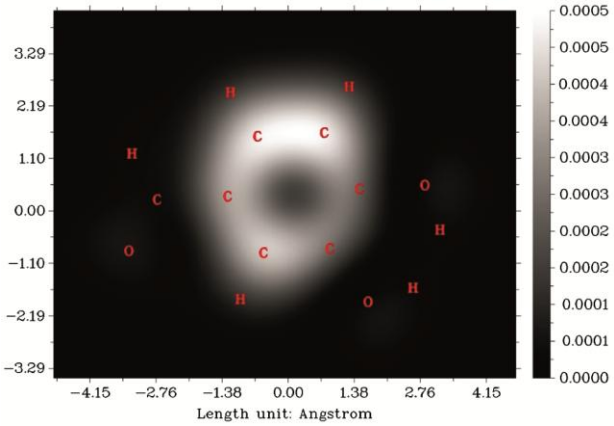

Fig. 11 — STM image for the title molecule

π→π* transition, and if it is below 0.8 a.u. it will undergo the n→π* transition. In these excitations, S0 → S3 (0.8199 a.u.), and S0 → S5 (0.8280 a.u.), S0 → S8 (0.8375 a.u.) undergo a π→π* transition since the values are larger than 0.8 a.u. Other excitations follow the n→π* transition.

The parameter H index shows the width of the average distribution of electrons and holes. The electron and hole map (Fig. 11) shows that the electrons and holes of S0 → S1, and S10 are dispersed over the small area. in order for their H index values to be small. Their H index values are higher because the spread of holes and electrons corresponding to the excitation from S0 → S6 and S7 is clearly broader.

The positive τ indices of S0 → S4, S9, and S10 indicate that the hole and electron separation is noticeable. Thus, the charge transfer (CT) kind of excitations are easily understood by everybody. The fact that the τ indices for the other excitations from S0 are unquestionably negative indicates that there is very little separation between the hole and the electron. They solely adhere to the local kind (LE) of excitation as a result.

The electron-hole The D index should be the primary factor in the relationship between the electron excitation characteristics and the coulomb attractive energy indicated in Table 10. The distance between the electron and hole main distributions increases with increasing D index, whereas the Coulomb energy decreases with increasing D index. When compared to other excitations, the statistics clearly show that the Coulomb attraction energy for S0 to S7 is the lowest (4.0999 eV).

Since the Δr values are substantial, it is implied that all of the excitations from S0 may have a significant CT character. The Δr value in the original research recommends a threshold of 2.0 Å to differentiate between LE and CT excitations. However, S4, S9, and S10 exclusively follow the CT kind of stimulation and have positive τ values. The LE kind of excitation is followed by the other excitations.

It is obvious that the Lambda (Λ) value is closely inversely proportional to the Δr values. In general, the hole-electron separation distance decreases with increasing hole-electron overlapping extent. Here, Λ value of 0.1793 Å, which is obtained for the S0 → S7 excited states, is shorter. Through the analysis of the above isosurface maps (Fig. 11) and Table 10, the following assumptions are made:

S0→S1 LE type of excitation of n-π*
S0→S2 LE type of excitation of n-π*
S0→S3 LE type of excitation of π-π*
S0→S4 CT type of excitation of n-π*
S0→S5 LE type of excitation of π-π*
S0→S6 LE type of excitation of n-π*
S0→S7 LE type of excitation of n-π*
S0→S8 LE type of excitation of π-π*
S0→S9 CT type of excitation of n-π*
S0→S10 CT type of excitation of n-π*

Simulated scanning tunnelling microscope (STM) analysis

A scanning tunnelling microscope (STM) is a mammoth method to confirm the spatial variations of the tunnelling current in the junction between a sharp metallic tip and a conducting robe surface[54]. The Multiwfn 3.8 program is used to build and analyze the simulated scanning tunneling microscope picture for the title molecule, which is seen in Fig. 11. The local density of states (LDOS) value for the headline molecule is determined as 0.0005 a.u. at V = -3.5 V and Z = 2.2 Å. The bigger the LDOS and, consequently, the stronger the tunneling current (I), the brighter the white on this chart. According to the Tersoff-Hamann model, LDOS is positively proportional to "I." It is evident that the "I" signal is more noticeable than other atoms over the six-membered aromatic ring.

Molecular Docking Studies

In silico Prediction of activity spectra for substance (PASS)

The title compound's activity is predicted using the PASS online tool. It clearly predicts the activity spectrum of the compounds as probability activity (Pa) and probable inactivity (Pi). The ratio varies between 0.000 and 1.000. If the value of Pa > 0.7, it has a high probability of pharmacological action, and if 0.5 < Pa < 0.7, the probability is less. If Pa is less than 0.5, the compound has no pharmacological action[55]. The PASS analysis is generally carried out before docking studies to find out the better choice of protein. For the headline molecule, the Pa value is found to be 0.954, which is related to the aldehyde oxidase inhibitor enzyme.

Therefore, the human aldehyde dehydrogenase protein, which causes Asian Flush Syndrome, is chosen to be used in the docking investigations. It impacts 8% of the global population[56] and 35%–40% of East Asians. Therefore, it is agreed to use 6TGW, which is derived from Homo sapiens, to conduct the investigation.

Preparation of protein

The protein data bank (https://www.rcsb.org/structure/6TGW) provides the X-ray crystal structure of the human aldehyde dehydrogenase receptor (PDB ID: 6TGW). The Discovery Studio 4.1 Visualizer program (https://discover.3ds.com/discovery-studio-visualizer-download) is used to build the protein's structure prior to the molecular docking procedure. To render the complex receptor ligand-free, the protein is stripped of its water molecules and tiny ligands, such as heteroatoms. Polar hydrogen atoms are included in the protein, which is an essential and crucial process for the computation of atomic charges. The force field applied is CHARMm, and the partial charge applied is Momany-Rone. Finally, the protein is subjected to energy minimization. The Ramachandran plot is analysed for the prepared protein, and it is found that all the residues are within the expected range (98.08%) (https://zlab.umassmed.edu/bu/rama/index.pl).

Preparation of ligand

The title molecule's 2D structure is created using the Chemsketch tool (https://www.acdlabs.com/resources/free-chemistry-software-apps/chemsketch-freeware/) and saved as a.mol file. The Avogadro tool (https://avogadro.cc/) is then used to transform the 2D structure into an energy-minimized 3D structure and save it as a.pdb file. The process of optimisation is very important for a ligand molecule. It leads to a stable conformation of coordinates with minimum energy. The force field applied is the MMEF94 with the steepest descend algorithm. The SwissADME (http://www.swissadme.ch/index.php) online tool is used to verify the ligand's different characteristics for the Lipinski Rule of Five, and the results are shown in Table 11. It is evident from Table 11 that this molecule complies with the Veber, Egan, and Lipinski rules of the Five hypotheses.

Table 11 — Various physical properties of the Ligand

1	Molecular formula	$C_7H_6O_3$
2	Molecular weight	138.12 /mol
3	Number of hydrogen acceptors	3
4	Number of hydrogen bond donors	2
5	Number of rotatable bonds	1
6	Log $P_{o/w}$ (iLOGP)	0.79
7	Log $P_{o/w}$ (XLOGP3)	1.09
8	BBB permeant	yes
9	GI absorption	High
10	Lipinski Drug likeness	Yes
11	Veber Drug likeness	Yes
12	Egan Drug likeness	Yes
13	Bio-availability score	0.55
14	Synthetic accessibility	1.00

Docking studies

PyRx is a powerful tool that can be used for docking ligands with proteins[21]. The ligand under investigation is docked with the prepared 6TGW, and the results are analysed with the Discovery Studio 4.1 Visualizer software. Between the ligand and the protein, two strong hydrogen bonds are formed. The docking details are shown in Table 12. The hydroxyl group, which is in *para*-position with the aldehyde group, is attached to THR 140 with a bond distance of 2.58 Å, while the oxygen atom in the aldehyde group is attached to ARG A:139 with a bond distance of 2.22 Å. The docking score was found to be -5.5 kcal/mol. It clearly recommends that the ligand fit well with the protein. The docking pattern (3D and 2D) is viewed by Discovery Studio 4.1 Visualizer software and is shown in Fig. 12.

Toxicity analysis

The toxicity of 3,4-dihydroxybenzaldehyde is analyzed *in-silco* using EPA DSS TOX[22]. LC_{50} analyses were carried out *in-silico* in *Pimephales promelas* (Fathead minnow) and *Daphnia Magna* for 96 hours and 48 hours, respectively. Also, IGC_{50} in *T. pyriformis in silico* for 48 hours and LD_{50} in *Mus musculus*. The results showed that the values for LC_{50} in *Pimephales promelas* at 96 hours

Table 12 — Docking results and hydrogen bond interaction of the ligand with 6TGW

PDB ID	Binding affinity (kcal/mol)	No. of hydrogen bonds appeared	Hydrogen bond distance (Å)	Atom of ligand	Residue of protein
6TGW	–5.5	2	2.22	Oxygen	ARG A:139
			2.58	Oxygen	THR A:140

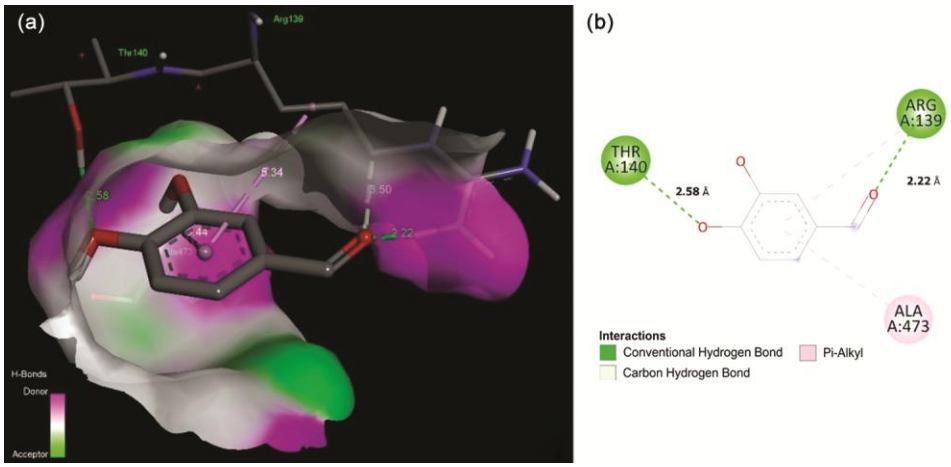

Fig. 12 — The docking pattern of the ligand with 6TGW protein

falls between 3.983 – Log_{10} (mol/L) to 14.373 mg/L and for *Daphnia Magna* at 48 hours falls between 4.148 – Log_{10} (mol/L) to 9.818 mg/L. The hierarchical clustering for both the organisms are also falling between 4.577 – Log_{10} (mol/L) and 3.660 mg/L and 3.740 – Log_{10} (mol/L) to 25.108 mg/L, respectively[57].

Regarding single model analysis, the values are 3.334 -Log_{10} (mol/L) to 6.954 mg/L and 4.546 – Log_{10} (mol/L) to 3.926 mg/L respectively. The group contribution and nearest neighbour too showed values from 4.006 – Log_{10} (mol/L) to 13.611 mg/L (taking their minimum to maximum into consideration). The results are also in line with the analysis, which showed a mild toxic effect on seizure threshold, lungs, and thorax[58].

With regard to the IGC_{50} using *T.pyriformis* at 48 hours duration showed that the experimental values fall between 3.107 - Log_{10} (mol/L) and 107.966 mg/L, also consensus with 3.201 – Log_{10} (mol/L) to 84.193 mg/L, and hierarchical clustering, group contribution and nearest neighbour with 3.162 – Log_{10} (mol/L) to 95.102 mg/L, 3.341 – Log_{10} (mol/L) to 63.001 mg/L and 3.142 – Log_{10} (mol/L) to 99.607 mg/L, respectively. Thus, the title compound seems to be less toxic. These results are similar to the results predicted by[59].

The oral LD_{50} analysis of the *Mus musculus* model showed that the title compound is more or less non-toxic in mammals. Having been with 2.113 – Log_{10} (mol/kg) to 1063.961 mg/kg and 2.141 – Log_{10} (mol/kg) to 998.230 mg/kg for consensus and hierarchical clustering, respectively. The nearest neighbour too showed a huge value ranging from 2.086 – Log_{10} (mol/kg) to 1134.022 mg/kg, which proposed that the toxicity level is very low or negligible to be considered. As per the factsheet of the MSDS, which synthesise this compound for commercial purpose, they list a possibility for mild eye, skin and respiratory irritations, which is in line with the analysis done[60].

The developmental toxicity is false for most cases bearing neighbourhood analysis that showed little toxicity. Regarding its Ames mutagenicity, the values showed a false nature for all the organisms. This compound may bind with the Estrogen Receptor, so it could have the tendency to show low reproductive toxicity. The word low could be signified because of its false nature in binding analysis using the nearest neighbour algorithm.

On a cumulative analysis, the title compound could be less toxic or no toxic to be considered. However, it could be toxic for lower organisms like planktons and fish. For most higher organisms, like mammals, it may pose a low toxicity and that is because of its reproductive interference due to Estrogen binding capacity[61].

PASS analysis

The applications are considered when the *Pa* value seems to be above 70%. A plot of comparison using *Pa* and *Pi* values (Fig. 13a) shows that most of the activity with high *Pa* values shows lesser *Pi* and thus the accuracy of the prediction. Regarding the frequency of prediction, the *Pa* value of 0.8 and its nearest values were more exhibited for most of the metabolic reactions, and so it is found to be accurate or moderately accurate (Fig. 13b). More the value nearer to 1 seems more towards perfection[62]. With the help of the PASS online server, the metabolic linkages of the title molecule are predicted. The results obtained from the PASS online server are subjected to retrieval of secondary information, as shown in Supplementary file and ST3[23]. Broadly, the reactions are categorized as metabolic pathways, environmental applications, plant interactions, natural flavours, diseases, and other medical applications, *etc*.

The title compound is predicted to be reactive in many metabolic pathways (16 Nos.), primarily with its core interactions pertaining to about 26 reactive

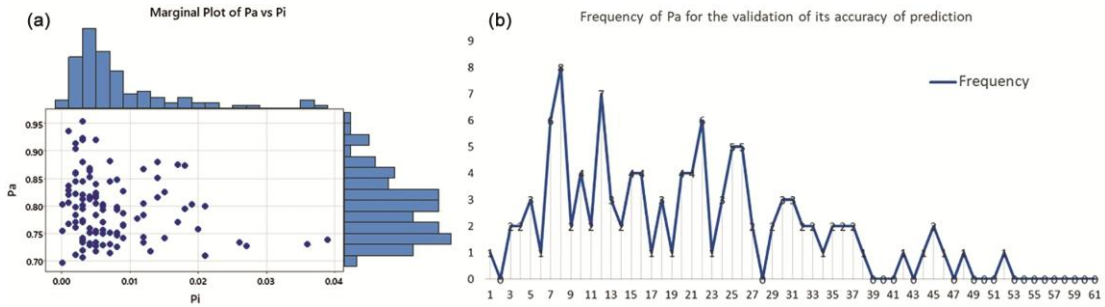

Fig. 13 — (a) Marginal plot of Pa Vs Pi (b) The Frequency of Pa for the validation of its accuracy of prediction

domains of serious metabolic enzymes. It is assumed that the compound is highly reactive to cytochrome proteins, fatty acid metabolism, alcohol metabolism, protein synthesis, *etc*. and is an antioxidant with about 11 different enzyme systems contributing to the xenobiotic degradation activity. About 25 enzymes, with their metabolic activity identified, are predicted to be anti-cancerous in nature.

The headline compound also interacts well with the plant systems (4 Nos) *in silico*, which aids its help in calcium metabolism, plant growth regulators, and secondary metabolite synthesis, and nitrogen metabolism. Also, its contribution may be extended to environmental applications (2 Nos), *viz*. insect repellent and bio-remediation. It could also be a natural flavour.

The molecule may also found to be sensitive medically and could be used to treat various ailments (18 Nos). It is proposed to be anti-cancerous and is against prostate cancer, breast cancer, hepatic cancer, colorectal cancer, stomach cancer, renal cell cancer, leukaemia, skin cancer, and lung cancer, *etc*. It is also predicted for controlling various cancers pertaining to about 47 metabolic activities and help in angiogenesis and anti-metastatic therapy[63].

This compound may be an antagonist to cardiovascular diseases, involving about nine enzymatic reactions. It is also considered against stroke, various respiratory problems, including tuberculosis, nervous disorders, gastro-intestinal infections, eye infections, arthritis, blood-related issues, kidney protective, immune-modulator, *etc*. It is proposed to be antagonistic for various diseases, *viz*, Alzheimer disease, Parkinson disease, Huntington's disease, MELAS syndrome, multiple sclerosis, Coffin-Lowry syndrome, Sjogren-Lansson's syndrome, *etc*. The activities pertaining to the ailments-related enzyme system are identified with the maximum percentage of activity scores.

There are also other medical applications vastly noted in the title compound, *viz*. kidney disorders (5), hepato-protective (14), anaesthetics (2), psychiatric (9), anti-microbial (10), anti-analgestic (1), anti-pyretic (1), anti-inflammatory (6), anti-diabetic (7), anti-toxic (5), immunological disorders (5), skin disorders (5), reproductive disorders (1), muscular disorders (2), biomarker (1), biosensor (1), anti-ageing (1), and sexual inducers (2). In comparison with the literature, the title compound is also a naturally available phenolic substance found in *Amomi fructus* and is also found to be anti-allergic, and anti-cancerous. It has also weakened the release of proteins associated with pro-inflammatory cytokines, TNF-α, and IL-6 genes in human mast cells[63].

In conclusion, this compound was found to possess more activities in *in silico* analysis. It is found to be less toxic and more reactive. It could be considered for further research to find its activity *in vitro* and *in vivo* so as to consider it as a drug resource.

Supplementary Information

Supplementary information is available in the website https://nopr.niscpr.res.in/handle/123456789/58776.

Acknowledgement

For providing the computer and software facilities, the authors are grateful to the Principal, Secretary, and administration of St. John's College, Palayamkottai.

Conclusion

Protocatechualdehyde is a naturally occurring polyphenol which is available in barley, Cavendish banana, *etc*. It has anti-oxidant properties too. The DFT/B3LYP/6-311++G(d,p) method is adopted to interpret the results. Mulltiwfn 3.8 is also used to find some physical properties. The electronic structure is determined. According to MEP analysis, both electrophilic and nucleophilic attacks are possible in this molecule. The FMO calculation result reveals that this is a stable and hard molecule. Experimental and theoretical studies for IR and UV-Vis are carried out, and their results are compared. The E(2) values developed by NBO analysis suggest that this molecule is very stable. The NCI study reveals that this molecule has an intramolecular hydrogen bond, van der Waals force, and steric factors. A shaded surface map with a projection of LOL analysis interprets that this molecule has electron depletion and electron-rich domains. Fukui function analysis tells about the electrophilic and nucleophilic attacking areas. The NHO study is done to fine the deviation. The hole-electron transfer study implies that charge transfer (CT) is possible at S0→S4, S9 and S10. The other excitations follow a local type of excitation only. STM analysis is studied for the title molecule. The ligand molecule is docked with the 6TGW protein. Through DSS TOX and PASS analysis, the title compound is predicted to be less or negligible toxic, and the results obtained are in line with the literature.

Funding

No specific grant was given to this research by funding organisations in the public, private, or not-for-profit sectors.

Conflict of interest

The authors state that they do not have any known competing financial interests or personal ties that could appear to have influenced the work disclosed in this study.

References

1 Choi J, Jiang X, Jeong J B & Lee S H, *J Med Food*, 17 (2014) 842.
2 Etoh H, Murakami K, Yogoh T, Ishikawa H, Fukuyama Y & Tanaka H, *Biosci Biotech Biochem*, 68 (2004) 2616.
3 Mulvena D, Webb E C& Zerner B, *Phytochem*, 8 (1969) 393.
4 Weber B, Hoesch L&Rast D M, *Phytochem*, 40 (1995) 433.
5 Kim M A, Kim E L, Kim K J, Hong J, Bao B &Jung J H, *Bull Korean Chem Soc*, 31 (2010) 1779.
6 Jeong J B & Lee S H, *Biochem Biophy Res Comm*, 430 (2013) 381.
7 Li S, Yu Y, Chen J, Guo B, Yang L & Ding W, *Molecules*, 21 (2016) 754.
8 Kong B S, Cho Y H & Lee E J, *PLoS One*, 20 (2014) e113242.
9 Wei Z F, Ni L J, Quana H & Duan J, *RSC Adv*, 11 (2021) 16955.
10 Azizi N, Heidarzadeh F & Farzaneh F, *Appl Organomet Chem*, 35 (2021) e6373.
11 Alharis R A, Al-Asadi R H & Hassan D A, *Egypt J Chem*,64 (2021) 5755.
12 Gaussian 16, Revision C01, Frisch M J, Trucks G W, Schlegel H B, Scuseria G E, Robb M A, Cheeseman J R, Scalmani G, Barone V, Petersson G A, Nakatsuji H, Li X, Caricato M, Marenich A V, Bloino J, Janesko B G, Gomperts R, Mennucci B, Hratchian H P, Ortiz J V, Izmaylov A F, Sonnenberg J L, Williams-Young D, Ding F, Lipparini F, Egidi F, Goings J, Peng B, Petrone A, Henderson T, Ranasinghe D, Zakrzewski V G, Gao J, Rega N, Zheng G, Liang W, Hada M, Ehara M, Toyota K, Fukuda R, Hasegawa J, Ishida M, Nakajima T, Honda Y, Kitao O, Nakai H, Vreven T, Throssell K, Montgomery J A, Jr Peralta J E, Ogliaro F, Bearpark M J, Heyd J J, Brothers E N, Kudin K N, Staroverov V N, Keith T A, Kobayashi R, Normand J, Raghavachari K, Rendell A P, Burant J C, Iyengar S S, Tomasi J, Cossi M, Millam J M, Klene M, Adamo C, Cammi R, Ochterski J W, Martin R L, Morokuma K, Farkas O, Foresman J B, Fox D J, Gaussian, Inc, Wallingford CT, (2016)
13 Becke A D, *J Chem Phys*, 98 (1993)5648.
14 Lee C, Yang W X & Par R G, *Phys Rev*, 37B (1988)785.
15 ACD/ChemSketch, version 2020.2.1, (Advanced Chemistry Development, Inc., Toronto, ON, Canada), 2021. www.acdlabs.com.
16 Hanwell M D, Curtis D E, Lonie D C, Vandermeersch T, Zurek E & HutchisonG R, *J Cheminfo*, 4 (2012) 17.
17 GaussView, Version 6.1, Roy Dennington, Todd A Keith, and John M Millam, Semichem Inc., Shawnee Mission, KS, (2016).
18 O'Boyle N M, Tenderholt A L &Langner K M, *J Comp Chem*, 29 (2008) 839.
19 Lu T & Chen F, *J Comp Chem*, 33 (2012) 580.
20 Humphrey W, Dalke A & Schulten K, *J Mol Graph*, 14 (1996) 33.
21 Dallakyan S & Olson A J, *Meth Mol Biol*, 1263 (2015) 243.
22 Distributed Structure-Searchable Toxicity (DSSTox) Database, US EPA, *US EPA*, www.epa.gov. https://www.epa.gov/chemical-research/distributed-structure-searchable-toxicity-dsstox-database (2015).
23 Lagunin A, Stepanchikova A, Filimonov D & Poroikov V, *Bioinfo*, 16 (2000) 747.
24 Balachandran V & Karpagam V, *J Mole Struc*, 1038 (2013) 52.
25 Hong L X, Ru L X & Zhou Z X, *Comp Theor Chem*, 969 (2011) 27.
26 Joshi B D, Srivastava A, Tandon P & Jain S, *Spectrochim Acta Part A: Mol Biomol Spectr*, 82 (2011) 270.
27 Saravanan S & Balachandran V, *Spectrochim Acta Part A: Mol Biomol Spect*, 138 (2015) 406.
28 Fukuli K, Yonezawa T & Shingu H, *J Phys Chem*, 20 (1952)722.
29 Gunasekaran S, Balaji R A, Kumaresan S, Anand G & Srinivasan S, *Canadian J Anal Sci Spect*, 53 (2008) 149.
30 Kores J J, Danish I A, Sasitha T, Stuart J G, Pushpam E J & Jebaraj W, *Heliyon*,7 (2021) e08377.
31 Kurt M & Yurdakul S, *J Mol Struc (Theochem)*, 730 (2005) 59.
32 Misra N, Prasad O, Sinha L & Pandey A, *J Mol Struc (Theochem)*, 822 (2007) 45.
33 Jamróz M H, *Spectrochim Acta Part A: Mole Biomole Spec*, 114 (2013) 220.
34 Clothup N B,Daly L H & Wiberley S E, *Introduction to Infrared and Raman Spectroscopy*, (Academic Press, New York), 1990.
35 Krishnakumar V & Balachandran V, *Indian J Pure Appl Phys*, 7 (2009) 823.
36 Singh H J & Srivastava P, *Indian J Pure Appl Phys*, 47 (2009) 557.
37 Mohan J, *Organic Spectroscopy – Principle and Applications, second ed.*, (Narosa Publishing House, New Delhi), 2001.
38 Krishnakumar V & Balachandran V, *Spectrochim Acta Part A*, 63 (2006) 464.
39 Scocrates G, *Infrared and Raman Characteristic Group Wave Number – Tables and Charts, third ed.*, (Wiley, New York), 2001.
40 Karunakaran V, Balachandran V, *Spectrochim Acta Part A, Mol Biomol Spect*, 98 (2012) 229.
41 Szafran M, Komasa A & Adamska E B, *J Mol Struc (Theochem)*, 827 (2007) 101.
42 James C, Raj A A, Reghunathan R, Jayakumar V S & Joe I H, *J Raman Spect*, 37 (2006)1381.
43 Liu J N, Chen Z R & Yuan S F, *J Zhejiang Univ Sci B*, 6 (2005) 584.
44 Kavitha E, Sundaraganesan N, Sebastian S & Kurt M, *Spectrochim Acta Part A Mol Biomol Spect*, 77 (2010) 612.
45 Bandyopadhyay A P, Karmakar A.Deb J, Sarkar U, & Md Seikh M, *Spectrachim Acta Part A*, 228 (2019) 117827.
46 Lu T & Chen F, *J Comp Chem*, 33 (2012) 580
47 Schmider H L & Becke A D, *J Mol Struc: (TheoChem)*, 527 (2000) 51.
48 Parr R G & Yang W, *Functional Theory of Atoms and Molecule*, (Oxford University Press, New York), 1989.

49 Ayers P W & Parr R G, *J Am Chem Soc*, 122 (2002) 2010.
50 Parr R G &Yang W J, *Am Chem Soc*, 106 (1984) 511.
51 Morell C, Grand A & Toro-Labbe A, *J Phys Chem A*, 109 (2005) 205.
52 NBO Version 3.1, Glendening E D, Reed A E, Carpenter J E & F Weinhold, Liu Z, Lu T & Chen Q, *Carbon*, 165 (2020) 461
53 Donner B, Kleber M, Bracher C & Kreuzer H J, *Am J Phys*, 73 (2005) 690.
54 Butina D, Segall M D & Frankcombe K, *Drug Disc To*, 7 (2002) S83.
55 Matsumura Y, Stiles K M, Reid J, Frenk E Z, Cronin S, Pagovich O E & Crystal R G, *Mol Ther Meth Clin Dev*, 26 (2019) 72.
56 McEachran A D, Balabin I, Cathey T, Transue T R, Al-Ghoul H, Grulke C, Sobus J R & Williams A J, *Sci Data*, 6 (2019) 141.
57 Caujolle F, Meynier D & Amin M, *Ann Pharm Fr*, 15 (1957) 461.
58 Luan F, Wang T, Tang L, Zhang S & Cordeiro M N D S, *Molecules*, 23 (2018) 1002.
59 Cdhfinechemical.com 2022 Material safety data sheet 3,4-dihydroxybenzaldehyde CAS No 139-85-5 https://www.cdhfinechemical.com/images/product/msds/10_1057720121_3,4-Dihydroxybenzaldehyde-CAS no-139-85-5-MSDS.pdf.
60 Sourkes T l, Sloane S B & Drujan B D, *AMA Arch Neuro Psy*, 78 (1957)204.
61 Adnan M, Chy M N U, Kamal A T M M, Chowdhury K A A, Rahman M A, Reza A S M A, Moniruzzaman M, Rony S R, Nasrin M S, Azad M O K, Park C H, Lim Y S & Cho D H, *Biomolecules*, 10 (2020) 561.
62 Choi H G, Je I G, Kim G J, Choi H, Kim S H, Kim J.A & Lee K S, *Nat Prod Commun*, 10(4) (2015) 631